JOURNAL OF THERMOPHYSICS AND HEAT TRANSFER
Vol. 19, No. 2, April–June 2005

Fluid Flow Around and Heat Transfer from Elliptical Cylinders: Analytical Approach

W. A. Khan,* J. R. Culham,† and M. M. Yovanovich‡
University of Waterloo, Waterloo, Ontario N2L 3G1, Canada

An integral method of boundary-layer analysis is employed to derive closed-form expressions for the calculation of total drag and average heat transfer for flow across an elliptical cylinder under isothermal and isoflux thermal boundary conditions. The Von Kármán–Pohlhausen integral method is used to solve the momentum and energy equations for both thermal boundary conditions. A fourth-order velocity profile in the hydrodynamic boundary layer and a third-order temperature profile in the thermal boundary layer are used. The present results are in good agreement with existing experimental/numerical data and, in the limiting cases, can be used for circular cylinders and finite plates.

Nomenclature

a	=	semimajor axis of elliptical cylinder, m
b	=	semiminor axis of elliptical cylinder, m
C_D	=	total drag coefficient
C_{D_f}	=	friction drag coefficient
C_{D_p}	=	pressure drag coefficient
C_f	=	skin friction coefficient, $\equiv 2\tau_w/\rho U_{\text{app}}^2$
C_p	=	pressure coefficient, $\equiv 2\Delta p/\rho U_{\text{app}}^2$
c	=	dimensional focal distance, m
c_p	=	fluid specific heat, kJ/kg K
D	=	diameter of circular cylinder, m
$E(e)$	=	complete elliptic integral of second kind
e	=	eccentricity, $\equiv \sqrt{(1-\epsilon^2)}$
g_{11}, g_{22}	=	metric coefficients
$\bar{h}$	=	average heat-transfer coefficient, W/m^2 K
k	=	thermal conductivity, W/m K
L	=	length of finite plate, m
$\mathcal{L}$	=	characteristic length $\equiv 2a$, m
$Nu_{\mathcal{L}}$	=	Nusselt number based on characteristic length $\equiv \mathcal{L}\bar{h}/k_f$
P	=	pressure, N/m^2
Pr	=	Prandtl number $\equiv \nu/\alpha$
q	=	heat flux, W/m^2
$Re_{\mathcal{L}}$	=	Reynolds number based on characteristic length $\equiv \mathcal{L}U_{\text{app}}/\nu$
r	=	radius of curvature of surface, m
s	=	distance along curved surface of elliptical cylinder measured from forward stagnation point, m
T	=	temperature, °C
U_{app}	=	approach velocity, m/s
$U(s)$	=	velocity in inviscid region just outside boundary layer, m/s
u	=	s-component of velocity in boundary layer, m/s
v	=	η-component of velocity in boundary layer, m/s
x, y	=	Cartesian coordinates
δ	=	hydrodynamic boundary-layer thickness, m
δ_1	=	displacement thickness, m
δ_2	=	momentum thickness, m
δ_T	=	thermal boundary layer thickness, m
ϵ	=	axis ratio $\equiv b/a$
η	=	distance normal to and measured from surface of elliptical cylinder, m
θ	=	angle measured from stagnation point, radians
λ	=	pressure gradient parameter
μ	=	absolute viscosity of fluid, kg/ms
ν	=	kinematic viscosity of fluid, m^2/s
ξ, θ	=	modified polar coordinates
ρ	=	fluid density, kg/m^3
τ	=	shear stress, N/m^2

Subscripts

a	=	ambient
f	=	fluid
p	=	pressure
s	=	separation
T	=	thermal
w	=	wall

Received 28 April 2004; presented as Paper 2004-2272 at the AIAA 37th Thermophysics Conference, Portland, OR, 28 June–1 July 2004; revision received 5 July 2004; accepted for publication 8 July 2004.

*Postdoctoral Fellow, Department of Mechanical Engineering. Member AIAA.

†Associate Professor and Director, Microelectronics Heat Transfer Laboratory, Department of Mechanical Engineering.

‡Distinguished Professor Emeritus, Department of Mechanical Engineering. Fellow AIAA.

Introduction

MANY industrial applications, where heat loads are substantial and space is limited, require the use of tubular heat exchangers for the cooling of electronic equipment. In these applications, elliptical geometries outperform circular geometries. Elliptical cylinders offer less flow resistance and higher heat-transfer rates than circular cylinders. They provide more general geometrical configurations than circular cylinders. In the limiting cases, they represent a finite-length plate when the axis ratio $\epsilon \to 0$ and a circular cylinder when the axis ratio $\epsilon \to 1$. Thus, a systematic analytical investigation of elliptical geometries can provide flow and heat-transfer characteristics not only from elliptical cylinders of different axis ratios but also from circular cylinders and finite-length flat plates. Because of space limitations, existing literature is reviewed for the elliptical cylinders only.

There have been few experimental/numerical studies of fluid flow and heat transfer from elliptical cylinders. Schubauer[1,2] conducted experiments to determine velocity distributions in the laminar boundary layer on the surface of an elliptic cylinder with axis ratio 1:3. He found that the velocity distributions in the boundary layer, its thickness, and its tendency to separate from the surface of the body are governed almost entirely by the velocity distribution in the region of potential flow outside the boundary layer. He got good agreement with the approximate method, developed by Pohlhausen,[3] for the forward part of the cylinder. The same approximate method was used by Schlichting and Ulrich[4] to calculate

boundary-layer parameters for elliptical cylinders of different axis ratios, mentioned by Schlichting.[5]

Ota et al.[6,7] experimentally studied heat transfer and flow around elliptical cylinders of axis ratios 1:2 and 1:3. Their results show that the heat-transfer coefficient of an elliptical cylinder is higher than that of a circular one with equal circumference and the pressure drag coefficients of the former are much lower than those of the later. Žukauskas and Žiugžda[8] experimentally studied fluid flow and heat transfer from an elliptical cylinder with 1:2 ratio between minor and major axes and with air flow parallel to either axis. They found higher heat-transfer coefficients for elliptical cylinders.

Modi et al.[9] studied experimentally the aerodynamics of a set of two-dimensional, stationary elliptic cylinders with different axis ratios in the subcritical–Reynolds number range 3×10^3–10^5. They presented extensive results on static pressure distribution, Strouhal number, and near-wake geometry as functions of the angle of attack and Reynolds number. They also determined the separation points using the analytical Gortler series solution approach.

Kondjoyan and Daudin[10] measured experimentally the effect of freestream turbulence intensity on heat and mass transfer at the surfaces of a circular cylinder and an elliptical cylinder with axis ratio 1:4. They found that the effect of turbulence intensity appeared to be as important as the influence of velocity and seemed to be independent of the pressure gradient and of the degree of turbulence isotropy.

Jackson,[11] D'Allessio and Dennis,[12,13] and D'Allessio[14] numerically studied the flow of a viscous incompressible fluid past an inclined elliptic cylinder. They obtained solutions for Reynolds numbers up to 100 and for various inclinations. Good agreement was found with the existing results. Li et al.[15] experimentally showed that the heat-transfer rate with elliptical pin fins is higher than that with circular pin fins, whereas the flow resistance of the former is much lower than that of the latter in the Reynolds-number range from 10^3 to 10^4.

The results of these studies are applicable only over a fixed range of conditions. Furthermore, no analytical studies exist that provide closed-form solutions for fluid flow and heat transfer from elliptical cylinders for a wide range of axis ratio and Reynolds and Prandtl numbers. The following study will be used to derive closed-form expressions for the drag and heat-transfer coefficients from elliptical cylinders of arbitrary axis ratio. For the limiting cases, these expressions will be used for circular cylinders and finite plates. The basic parameters involved in this problem are the minor–major axis ratio, $\epsilon = b/a$, and the Reynolds and Prandtl numbers.

Analysis

Consider uniform flow of a Newtonian fluid past a fixed elliptical cylinder with major axis $2a$ and minor axis $2b$. The cylinder is oriented so that the major axis is parallel to the direction of the net flow in the main stream, thus making one end of the major axis a point of stagnation A (Fig. 1). The flow is assumed to be laminar, steady, and two-dimensional. The approach velocity of the air is U_{app} and the ambient temperature of the air is T_a. The surface temperature of the wall is T_w in the isothermal case and the heat flux is q for the isoflux case. The radius of curvature of the surface is r.

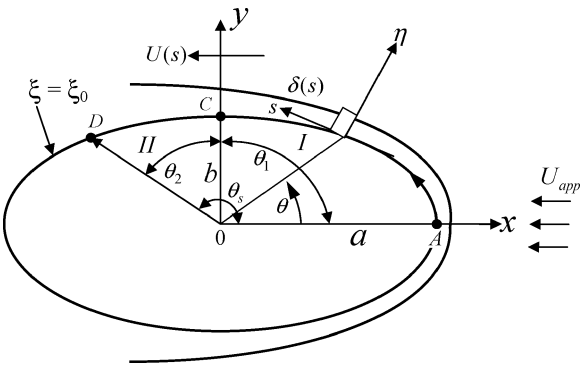

Fig. 1 Laminar flow over an elliptical cylinder.

For a comparison of total drag and heat transfer from an elliptical cylinder with those from a circular cylinder and a flat plate, a characteristic length is used in both the Reynolds and the Nusselt numbers. This characteristic length $\mathcal{L}$ is the equivalent diameter of a circular cylinder whose perimeter is the same as that of the elliptical cylinder and that of the flat plate. In this case, the distance traversed by the flow will be the same along the surfaces of the three objects. This length is

$$\mathcal{L} = 4aE(e)/\pi \tag{1}$$

where $E(e)$ is the complete elliptic integral of the second kind. In the limiting cases, when $\epsilon \to 1$, this characteristic length gives the diameter D of a circular cylinder, and when $\epsilon \to 0$, it represents the length L of a flat plate.

Coordinate System and Governing Equations

Following D'Allessio,[14] the mapping between Cartesian (x, y) and modified polar (ξ, θ) coordinates is

$$x = c\cosh\xi\cos\theta, \qquad y = c\sinh\xi\sin\theta \tag{2}$$

where c is the dimensional focal distance

$$c = a\sqrt{1-\epsilon^2} \qquad \text{with} \qquad \epsilon = b/a$$

The surface of an ellipse is defined by $\xi = \xi_0$, so that

$$\tanh\xi_0 = \epsilon \tag{3}$$

The elliptic coordinate system gives the metric coefficients

$$g_{11} = g_{22} = c\sqrt{\sinh^2\xi + \sin^2\theta} \tag{4}$$

The equations of continuity, momentum, and energy for steady-state forced convection of a Newtonian constant-property fluid with no heat generation can be expressed as

$$\nabla \cdot \boldsymbol{V} = 0 \tag{5}$$

$$\boldsymbol{V}\cdot\nabla\boldsymbol{V} = -(1/\rho)\nabla P + \nu\nabla^2\boldsymbol{V} \tag{6}$$

$$\boldsymbol{V}\cdot\nabla T = \alpha\nabla^2 T \tag{7}$$

where $\boldsymbol{V}$ is the velocity vector of the flowfield, ∇P is the pressure gradient for forced convection, and T is the temperature. For analyzing fluid flow around and heat transfer from an elliptical cylinder, it is convenient to use a curvilinear system of coordinates in which s denotes distance along the curved surface of the elliptical cylinder measured from the forward stagnation point and η is the distance normal to and measured from the surface (Fig. 1). In this system of coordinates, the velocity components in the local s- and η-directions are denoted by u and v. The potential flow velocity just outside the boundary layer is denoted by $U(s)$. Using an order-of-magnitude analysis, one can obtain the following simplified boundary layer equations corresponding to Eqs. (5–7):

Continuity

$$\frac{\partial u}{\partial s} + \frac{\partial v}{\partial \eta} = 0 \tag{8}$$

s-Momentum

$$u\frac{\partial u}{\partial s} + v\frac{\partial u}{\partial \eta} = -\frac{1}{\rho}\frac{\mathrm{d}P}{\mathrm{d}s} + \nu\frac{\partial^2 u}{\partial \eta^2} \tag{9}$$

η-Momentum

$$\frac{\mathrm{d}P}{\mathrm{d}\eta} = 0 \tag{10}$$

Energy

$$u\frac{\partial T}{\partial s} + v\frac{\partial T}{\partial \eta} = \alpha\frac{\partial^2 T}{\partial \eta^2} \tag{11}$$

Bernoulli equation

$$-\frac{1}{\rho}\frac{\mathrm{d}P}{\mathrm{d}s} = U(s)\frac{\mathrm{d}U(s)}{\mathrm{d}s} \tag{12}$$

Hydrodynamic Boundary Conditions

At the cylinder surface, $\eta = 0$,

$$u = 0, \qquad v = 0 \tag{13}$$

At the edge of the boundary layer, $\eta = \delta(s)$,

$$u = U(s), \qquad \frac{\partial u}{\partial \eta} = 0, \qquad \frac{\partial^2 u}{\partial \eta^2} = 0 \tag{14}$$

Thermal Boundary Conditions

The boundary conditions for the isothermal and isoflux cylinders are

$$\eta = 0, \begin{cases} T = T_w & \text{for uniform wall temperature (UWT)} \\ \dfrac{\partial T}{\partial \eta} = -\dfrac{q}{k_f} & \text{for uniform wall flux (UWF)} \end{cases} \tag{15}$$

$$\eta = \delta_T, \qquad T = T_a, \qquad \frac{\partial T}{\partial \eta} = 0 \tag{16}$$

Velocity Distribution

Assuming a thin hydrodynamic boundary layer around the cylinder, the velocity distribution in the boundary layer can be approximated by the fourth-order polynomial suggested by Pohlhausen[3] as

$$u/U(s) = \left(2\eta_H - 2\eta_H^3 + \eta_H^4\right) + (\lambda/6)\left(\eta_H - 3\eta_H^2 + 3\eta_H^3 - \eta_H^4\right) \tag{17}$$

where $\eta_H = \eta/\delta(s)$. This satisfies the boundary conditions (13) and (14). Outside the boundary layer, the velocity distribution may be approximated by the potential-flow solution[4]

$$U(s) = \frac{U_{\text{app}}(1+\epsilon)\sin\theta}{\sqrt{1 - e^2\cos^2\theta}} \tag{18}$$

Temperature Distribution

Assuming a thin thermal boundary layer around the cylinder, the temperature distribution in the thermal boundary layer can be approximated by the third-order polynomial

$$(T - T_a)/(T_w - T_a) = A + B\eta_T + C\eta_T^2 + D\eta_T^3 \tag{19}$$

where $\eta_T = \eta/\delta_T(s)$. Using the thermal boundary conditions (15) and (16), the temperature distribution is

$$(T - T_a)/(T_w - T_a) = 1 - \tfrac{3}{2}\eta_T + \tfrac{1}{2}\eta_T^3 \tag{20}$$

for the isothermal boundary condition and

$$T - T_a = (2q\delta_T/3k_f)\left(1 - \tfrac{3}{2}\eta_T + \tfrac{1}{2}\eta_T^3\right) \tag{21}$$

for the isoflux boundary condition.

Boundary-Layer Parameters

In dimensionless form, the momentum integral equation is written as

$$\frac{U(s)\delta_2}{\nu}\frac{\mathrm{d}\delta_2}{\mathrm{d}s} + \left(2 + \frac{\delta_1}{\delta_2}\right)\frac{\delta_2^2}{\nu}\frac{\mathrm{d}U}{\mathrm{d}s} = \frac{\delta_2}{U(s)}\frac{\partial u}{\partial \eta}\bigg|_{\eta=0} \tag{22}$$

where

$$\delta_1 = \delta\int_0^1 \left[1 - \frac{u}{U(s)}\right]\mathrm{d}\eta_H \tag{23}$$

$$\delta_2 = \delta\int_0^1 \frac{u}{U(s)}\left[1 - \frac{u}{U(s)}\right]\mathrm{d}\eta_H \tag{24}$$

Using the velocity distribution from Eq. (17), Eqs. (23) and (24) can be written as

$$\delta_1 = (\delta/10)(3 - \lambda/12) \tag{25}$$

$$\delta_2 = (\delta/63)(37/5 - \lambda/15 - \lambda^2/144) \tag{26}$$

Assuming that

$$Z = \frac{\delta_2^2}{\nu}, \qquad K = Z\frac{\mathrm{d}U}{\mathrm{d}s}$$

Equation (22) can be reduced to the nonlinear differential equation of the first order for Z,

$$\frac{\mathrm{d}Z}{\mathrm{d}s} = \frac{H(K)}{U(s)} \tag{27}$$

where $H(K) = 2f_2(K) - 2K[2 + f_1(K)]$ is a universal function and is approximated by Walz[16] by a straight line,

$$H(K) = 0.47 - 6K$$

with

$$f_1(K) = \frac{63(3 - \lambda/12)}{10(37/5 - \lambda/15 - \lambda^2/144)}$$

$$f_2(K) = \frac{1}{63}\left(2 + \frac{\lambda}{6}\right)\left(\frac{37}{5} - \frac{\lambda}{15} - \frac{\lambda^2}{144}\right)$$

$$K = \frac{\lambda}{3963}\left(\frac{37}{5} - \frac{\lambda}{15} - \frac{\lambda^2}{144}\right)^2 \tag{28}$$

Equation (27) can be solved for the dimensionless local momentum thickness,

$$\frac{\delta_2}{\mathcal{L}} = \frac{0.61}{\sqrt{Re_{\mathcal{L}}}}\sqrt{\frac{(1 - e^2\cos^2\theta)^3}{E(e)\sin^6\theta}\int_0^\theta \frac{\sin^5\theta\,\mathrm{d}\theta}{(1 - e^2\cos^2\theta)^2}} \tag{29}$$

Using the potential-flow velocity, Eq. (18), the dimensionless local boundary-layer thickness can be written as

$$\frac{\delta}{\mathcal{L}} = \frac{0.8862}{\sqrt{Re_{\mathcal{L}}}}\frac{(1 - e^2\cos^2\theta)}{\sqrt{\epsilon^2(1+\epsilon)E(e)}}\sqrt{\frac{\lambda}{\cos\theta}} \tag{30}$$

By solving Eqs. (26) and (30) and comparing the results with Eq. (29), the values of the pressure-gradient parameter λ corresponding to each position along the cylinder surface are obtained. These values are found to be positive from $0 \le \theta \le \theta_1 = 90$ deg (region I, bounded by AC0A) and negative from $\theta_1 \le \theta \le \theta_s$ (region II, bounded by C0DC), as shown in Fig. 1. Thus, the entire range of interest $0 \le \theta \le \theta_s$ can be divided into two regions and the λ values can be fitted separately by the least-squares method into two polynomials for each axis ratio.

Fluid Flow

The first topic of interest is fluid friction, which manifests itself in the form of the drag force F_D, which is the sum of the skin-friction drag D_f and pressure drag D_p. Skin-friction drag is due to viscous shear forces produced at the cylinder surface, predominantly in those regions to which the boundary layer is attached. The component of

shear force in the flow direction is given by

$$D_f = \int_s \tau_w \sin\theta \, \mathrm{d}A_s \tag{31}$$

where $\mathrm{d}A_s = \mathrm{d}s$ per unit length of cylinder. In the case of the elliptical geometry, the radial distance r to a point on the ellipse surface $\xi = \xi_0$ is

$$r = a\sqrt{1 - e^2\cos^2\theta} \tag{32}$$

Therefore, the length $\mathrm{d}s$ is

$$\mathrm{d}s = a\sqrt{1 - e^2\cos^2\theta}\,\mathrm{d}\theta \tag{33}$$

The shear stress on the cylinder wall τ_w can be obtained from Newton's law of viscosity. In dimensionless form, it can be written as

$$C_f = \frac{0.38\sqrt{\epsilon^2(1+\epsilon)^3 E(e)}}{\sqrt{Re_{\mathcal{L}}}} \frac{(\lambda + 12)\sin\theta}{(1 - e^2\cos^2\theta)^{\frac{3}{2}}} \sqrt{\frac{\cos\theta}{\lambda}} \tag{34}$$

The friction drag coefficient is defined as

$$C_{D_f} = \int_0^{\pi} C_f \sin\theta \, \mathrm{d}\theta = \int_0^{\theta_s} C_f \sin\theta \, \mathrm{d}\theta + \int_{\theta_s}^{\pi} C_f \sin\theta \, \mathrm{d}\theta \tag{35}$$

Because no shear stress acts on the cylinder surface after the boundary-layer separation, the second integral will be zero and the friction drag coefficient is written as

$$C_{D_f} = \int_0^{\theta_s} C_f \sin\theta \, \mathrm{d}\theta \tag{36}$$

The analytical definition for the boundary-layer separation shows that the separation point is characterized by zero transverse velocity gradient at the wall. The angle of separation θ_s calculated in this study depends upon the velocity distribution, Eq. (17), chosen inside the boundary layer. The angle of separation, for different axis ratios, is given in Table 1. It is important to note that these results follow the trend of Schlichting and Ulrich[4] and Schubauer[1] but do not confirm the Modi et al.[9] trend. The friction-drag coefficients are calculated for different axis ratios and a general correlation is deduced in terms of arbitrary axis ratio and Reynolds number:

$$C_{D_f} = \frac{1.353 + 4.43\epsilon^{1.35}}{\sqrt{Re_{\mathcal{L}}}} \tag{37}$$

In the limiting cases when $\epsilon \to 1$, this gives $5.783/\sqrt{Re_D}$ for a circular cylinder, and when $\epsilon \to 0$, it gives $1.353/\sqrt{Re_L}$ for a finite flat plate.

The pressure drag is due to the unbalanced pressures that exist between the relatively high pressures on the upstream surfaces and the lower pressures on the downstream surfaces. The component of pressure drag in the flow direction is given by

$$D_p = \int_s \Delta P \cos\theta \, \mathrm{d}A_s \tag{38}$$

Table 1 Angle of separation for different axis ratios of elliptical cylinder

ϵ	θ_s
1	1.88
0.9	1.91
0.8	1.95
0.6	2.05
0.5	2.12
0.4	2.21
0.3	2.31
0.2	2.45
0.1	2.65
0.01	2.99

which can be rewritten in terms of the pressure-drag coefficient as

$$C_{D_p} = \int_0^{\pi} C_p \cos\theta \sqrt{1 - e^2\cos^2\theta}\,\mathrm{d}\theta \tag{39}$$

The unbalanced pressure, $\Delta P = P_1 - P_2$, between upstream and downstream surfaces can be obtained by integrating the θ-component of Eq. (6) from P_1 to P_2. Using an order-of-magnitude analysis, the simplified θ-component of Eq. (6) in elliptic cylinder coordinates (ξ, θ) can be written as

$$\frac{u_\xi}{g_{11}}\frac{\partial u_\theta}{\partial \xi} + \frac{u_\theta}{g_{11}}\frac{\partial u_\theta}{\partial \theta} = -\frac{1}{g_{11}\rho}\frac{\partial P}{\partial \theta} + \frac{\nu}{g_{11}^2}\left\{\frac{\partial^2 u_\theta}{\partial \theta^2}\right\} \tag{40}$$

where g_{11} are the metric coefficients and are given by Eq. (4), u_ξ and u_θ are the velocity components in the ξ- and θ-directions and are given by

$$u_\xi = -\frac{1}{g_{11}}\frac{\partial \phi}{\partial \xi}, \qquad u_\theta = -\frac{1}{g_{11}}\frac{\partial \phi}{\partial \theta} \tag{41}$$

where ϕ is the potential function for a steady flow past an elliptical cylinder and is obtained from the complex potential

$$\phi = U_{\text{app}} a\sqrt{(1+\epsilon)/(1-\epsilon)}\cosh\xi\cos\theta(1 - \epsilon\tanh\xi) \tag{42}$$

Calculating the velocity components and their derivatives on the surface of the elliptic cylinder, one can find, from Eq. (38), the pressure coefficients for different axis ratios. These coefficients are then used, in Eq. (39), to determine the pressure-drag coefficients for different axis ratios. Using these coefficients, a general correlation in terms of the axis ratio and Reynolds number is found to be

$$C_{D_p} = (1.1526 + 1.26/Re_{\mathcal{L}})\epsilon^{0.95} \tag{43}$$

The total drag coefficient C_D can be written as the sum of both drag coefficients,

$$C_D = \frac{1.353 + 4.43\epsilon^{1.35}}{\sqrt{Re_{\mathcal{L}}}} + \left(1.1526 + \frac{1.26}{Re_{\mathcal{L}}}\right)\epsilon^{0.95} \tag{44}$$

In the limiting cases when $\epsilon \to 1$

$$C_D = 5.786\Big/\sqrt{Re_D} + 1.152 + 1.260/Re_D \tag{45}$$

for a circular cylinder and, when $\epsilon \to 0$, it gives

$$C_D = 1.353\Big/\sqrt{Re_L} \tag{46}$$

for a finite flat plate.

Heat Transfer

For the isothermal boundary condition, the energy integral equation can be written as

$$\frac{\mathrm{d}}{\mathrm{d}s}\int_0^{\delta_T}(T - T_a)u \, \mathrm{d}\eta = -\alpha\frac{\partial T}{\partial \eta}\bigg|_{\eta=0} \tag{47}$$

Using the velocity and temperature profiles, and assuming that $\zeta = \delta_T/\delta < 1$, Eq. (47) can be simplified to

$$\delta_T \frac{\mathrm{d}}{\mathrm{d}s}[U(s)\delta_T\zeta(\lambda + 12)] = 90\alpha \tag{48}$$

This equation can be rewritten separately as

$$\delta_T \frac{\mathrm{d}}{\mathrm{d}s}[U(s)\delta_T\zeta(\lambda_1 + 12)] = 90\alpha \tag{49}$$

for region I and

$$\delta_T \frac{\mathrm{d}}{\mathrm{d}s}[U(s)\delta_T\zeta(\lambda_2 + 12)] = 90\alpha \tag{50}$$

for region II. Multiplying both equations by $U(s)\zeta$ and integrating separately in the two regions, one can solve these two equations for the local thermal boundary-layer thicknesses to find

$$\left(\frac{\delta_T(\theta)}{\mathcal{L}}\right)\cdot Re_{\mathcal{L}}^{\frac{1}{2}}Pr^{\frac{1}{3}} = \sqrt{\frac{2.236}{(1+\epsilon)E(e)}} \times \begin{cases} \sqrt[3]{\dfrac{(1-e^2\cos^2\theta)^2 f_3(\theta)}{\epsilon(\lambda_1+12)^2\sin^2\theta}}\sqrt{\dfrac{\lambda_1}{\cos\theta}} & \text{for region I} \\ \sqrt[3]{\dfrac{(1-e^2\cos^2\theta)^2 f_5(\theta)}{\epsilon\sin^2\theta}}\sqrt{\dfrac{\lambda_2}{\cos\theta}} & \text{for region II} \end{cases} \quad (51)$$

where

$$f_3(\theta) = \int_0^\theta \sin\theta(\lambda_1+12)\,\mathrm{d}\theta \quad (52)$$

$$f_5(\theta) = \frac{f_3(\theta)}{\lambda_1+12} + \frac{f_4(\theta)}{\lambda_2+12} \quad (53)$$

with

$$f_4(\theta) = \int_{\theta_1}^{\theta_s} \sin\theta(\lambda_2+12)\,\mathrm{d}\theta \quad (54)$$

For the isothermal boundary condition, the local heat-transfer coefficient is

$$h(\theta) = -k_f\left.\frac{\partial T}{\partial\eta}\right|_{\eta=0}\Big/(T_w - T_a) = \frac{3k_f}{2\delta_T} \quad (55)$$

Thus, the local Nusselt numbers for both regions can be written as

$$\frac{Nu_{\mathcal{L}}(\theta)|_{\text{isothermal}}}{Re_{\mathcal{L}}^{\frac{1}{2}}Pr^{\frac{1}{3}}} = \frac{\sqrt{(1+\epsilon)E(e)}}{3.33} \times \begin{cases} \sqrt[3]{\dfrac{\epsilon(\lambda_1+12)^2\sin^2\theta}{(1-e^2\cos^2\theta)^2 f_3(\theta)}}\sqrt{\dfrac{\cos\theta}{\lambda_1}} & \text{for region I} \\ \sqrt[3]{\dfrac{\epsilon\sin^2\theta}{(1-e^2\cos^2\theta)^2 f_4(\theta)}}\sqrt{\dfrac{\cos\theta}{\lambda_2}} & \text{for region II} \end{cases} \quad (56)$$

The average heat-transfer coefficient is defined as

$$\bar{h} = \frac{1}{\pi}\int_0^\pi h(\theta)\,\mathrm{d}\theta = \frac{1}{\pi}\left[\int_0^{\theta_s} h(\theta)\,\mathrm{d}\theta + \int_{\theta_s}^\pi h(\theta)\,\mathrm{d}\theta\right] \quad (57)$$

It has been observed experimentally by many researchers that, at low Reynolds numbers, there is no appreciable increase in the local heat transfer after the separation point. However, at high Reynolds numbers, the local heat transfer increases from the separation point to the rear stagnation point. Hence, the average heat transfer coefficient is

$$\bar{h} = \frac{1}{\pi}\int_0^{\theta_s} h(\theta)\,\mathrm{d}\theta = \frac{1}{\pi}\left[\int_0^{\theta_1} h_1(\theta)\,\mathrm{d}\theta + \int_{\theta_1}^{\theta_s} h_2(\theta)\,\mathrm{d}\theta\right] \quad (58)$$

Using Eqs. (51–54), Eq. (58) can be solved for the average heat-transfer coefficient, which gives the average Nusselt number for an isothermal elliptical cylinder of arbitrary axis ratio ϵ as

$$\frac{Nu_D|_{\text{isothermal}}}{Re_{\mathcal{L}}^{\frac{1}{2}}Pr^{\frac{1}{3}}} = 0.75 - 0.16\exp\left(\frac{-0.018}{\epsilon^{3.1}}\right) \quad (59)$$

For the isoflux boundary condition, the energy integral equation can be written as

$$\frac{\mathrm{d}}{\mathrm{d}x}\int_0^{\delta_T}(T-T_a)u\,\mathrm{d}\eta = \frac{q}{\rho c_p} \quad (60)$$

For constant heat flux and thermophysical properties, Eq. (60) can be simplified to

$$\frac{\mathrm{d}}{\mathrm{d}s}\left[U(s)\delta_T^2\zeta(\lambda+12)\right] = 90\frac{\nu}{Pr} \quad (61)$$

Rewriting Eq. (61) for the two regions in the same way as Eq. (48), one can obtain the local thermal boundary layer thicknesses δ_{T_1} and δ_{T_2} under isoflux boundary condition. The local surface temperatures for the two regions can then be obtained from Eq. (21) as

$$\Delta T_1(\theta) = 2q\delta_{T_1}\big/3k_f \quad (62)$$

$$\Delta T_2(\theta) = 2q\delta_{T_2}\big/3k_f \quad (63)$$

The local heat transfer coefficient can now be obtained from its definition as

$$h_1(\theta) = q/\Delta T_1(\theta), \qquad h_2(\theta) = q/\Delta T_2(\theta) \quad (64)$$

Following the same procedure for the average heat-transfer coefficient, one can obtain the average Nusselt number for an isoflux cylinder as

$$\frac{Nu_{\mathcal{L}}|_{\text{isoflux}}}{Re_{\mathcal{L}}^{\frac{1}{2}}Pr^{\frac{1}{3}}} = 0.91 - 0.31\exp\left(\frac{-0.09}{\epsilon^{1.79}}\right) \quad (65)$$

This Nusselt number is 6% greater than the average Nusselt number for an isothermal circular cylinder. Combining the results for both thermal boundary conditions, we have

$$\frac{Nu_{\mathcal{L}}}{Re_{\mathcal{L}}^{\frac{1}{2}}Pr^{\frac{1}{3}}} = \begin{cases} 0.75 - 0.16\exp\left(\dfrac{-0.018}{\epsilon^{3.1}}\right) & \text{UWT} \\ 0.91 - 0.31\exp\left(\dfrac{-0.09}{\epsilon^{1.79}}\right) & \text{UWF} \end{cases} \quad (66)$$

which gives the dimensionless Nusselt numbers for elliptical cylinders of arbitrary axis ratio under isothermal or isoflux boundary conditions. In the limiting cases, when $\epsilon = 1$, it represents the average Nusselt numbers for a circular cylinder,

$$\frac{Nu_D}{Re_D^{\frac{1}{2}}Pr^{\frac{1}{3}}} = \begin{cases} 0.5930 & \text{UWT} \\ 0.6321 & \text{UWF} \end{cases} \quad (67)$$

And, when $\epsilon = 0$, it represents the average Nusselt number for a finite flat plate as

$$\frac{Nu_L}{Re_L^{\frac{1}{2}}Pr^{\frac{1}{3}}} = \begin{cases} 0.750 & \text{UWT} \\ 0.912 & \text{UWF} \end{cases} \quad (68)$$

where L is the length of the plate.

Results and Discussion

The dimensionless shear stress, $C_f\sqrt{Re_{\mathcal{L}}}$, at the surfaces of cylinders of different axis ratios is shown in Fig. 2. This shows that C_f is zero at the stagnation point for each case and reaches a maximum at a certain angle, which decreases with the axis ratio. The increase in shear stress is caused by the deformation of the velocity profiles in the boundary layer, a higher velocity gradient at the wall, and a thicker boundary layer. In the region of decreasing C_f preceding the separation point, the pressure gradient decreases further and finally C_f falls to zero at the separation angle which increases with the axis ratio. These angles in radians are presented in Table 1. Beyond the separation point, C_f remains close to zero up to the rear stagnation point.

The results for the circular cylinder are also shown in the same figure for comparison. The total drag coefficients versus axis ratio are plotted in Fig. 3 for different Reynolds numbers. It is clear that the total drag coefficient decreases from the circular cylinder to the

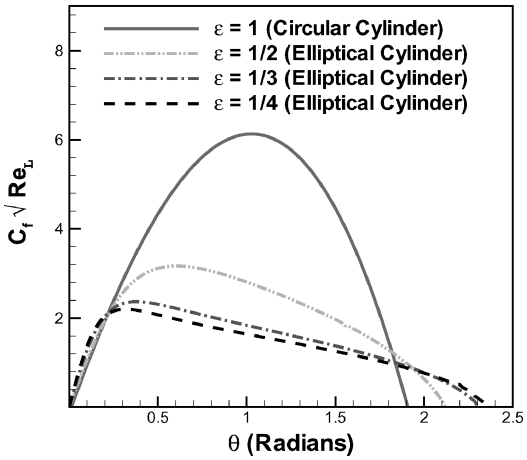

Fig. 2 Distribution of shear stress on surface of cylinders in air.

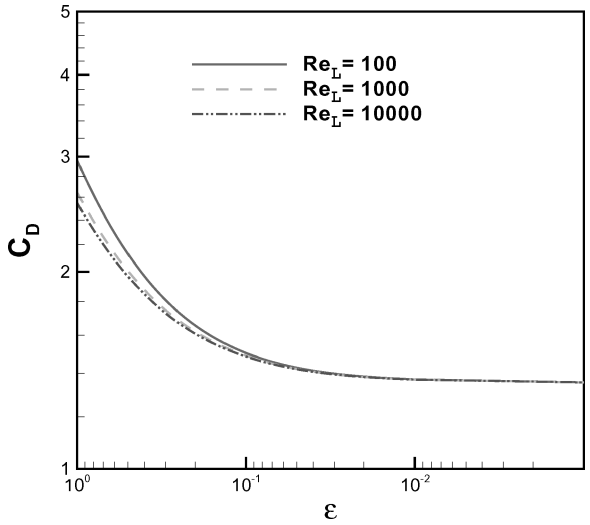

Fig. 3 Variation of total drag coefficient with axis ratio.

finite flat plate. For larger axis ratios, these coefficients depend upon the Reynolds numbers, but for smaller axis ratios, the coefficients are independent of Reynolds numbers. The total drag coefficients versus Reynolds numbers are shown in Fig. 4 for different axis ratios. As expected, the drag coefficients are highest for the circular cylinder and lowest for the flat plate.

The drag coefficients of the elliptical cylinder lie between these two limits and decrease with the Reynolds numbers. The present results for circular cylinder and finite flat plate are compared with the experimental data of Wieselsberger[17] and Janour,[18] respectively. It is clear that the present results are in good agreement with the experimental data. The friction drag coefficients of the finite flat plate, obtained from the present model, are also compared with the experimental[18] and numerical[19] data in Fig. 5. The theoretical correlations of Van Dyke[20] and Kuo[21] further confirm the present fluid flow model.

The heat-transfer parameter $Nu_{\mathcal{L}}/Re_{\mathcal{L}}^{1/2}Pr^{1/3}$ is plotted vs the axis ratio ϵ in Fig. 6. The curve shows that the heat-transfer parameter increases very slowly from the circular cylinder ($\epsilon = 1$) to a certain axis ratio ($\epsilon = 0.5$) and then increases rapidly up to ($\epsilon = 0.1$), and after that it becomes constant for the finite flat plate. The average Nusselt numbers of isothermal elliptic cylinders versus Reynolds numbers are presented in Fig. 7. It is clear that $Nu_{\mathcal{L}}$ increases linearly with $Re_{\mathcal{L}}$ on a log–log plot for all cases. Nusselt numbers for the circular cylinder are found to be lower than for any geometry considered in this study. The present results for the circular cylinder are compared with the empirical correlation of Churchill and Bernstein[22] and the finite flat-plate results are compared with the

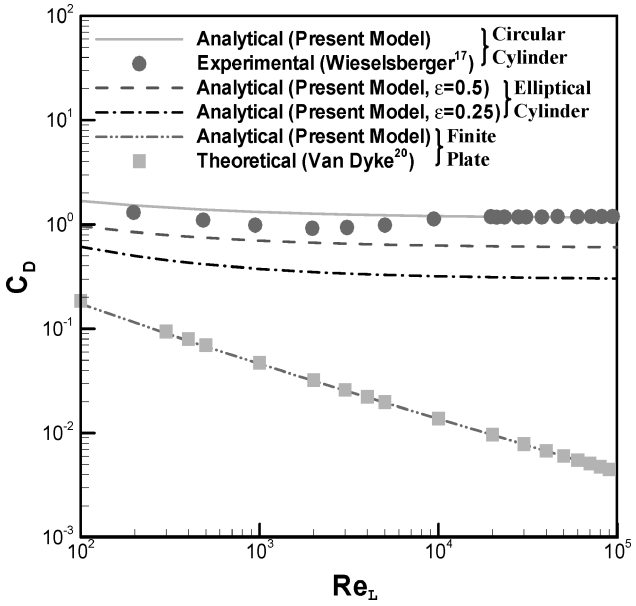

Fig. 4 Variation of total drag coefficient with Reynolds number.

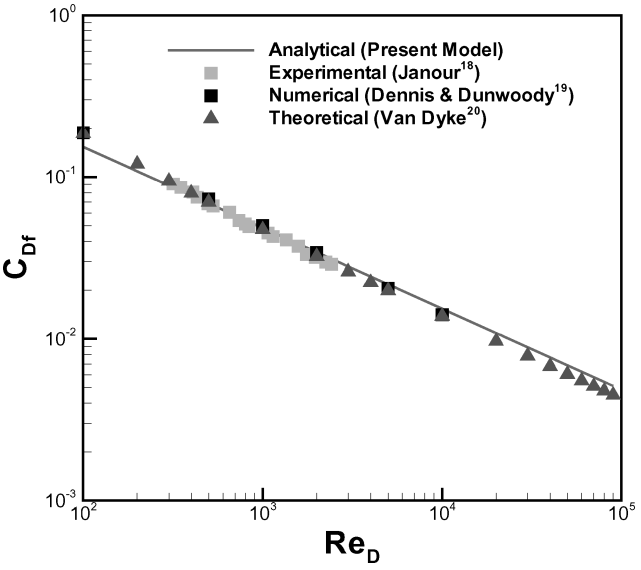

Fig. 5 Comparison of friction drag coefficients of a finite flat plate.

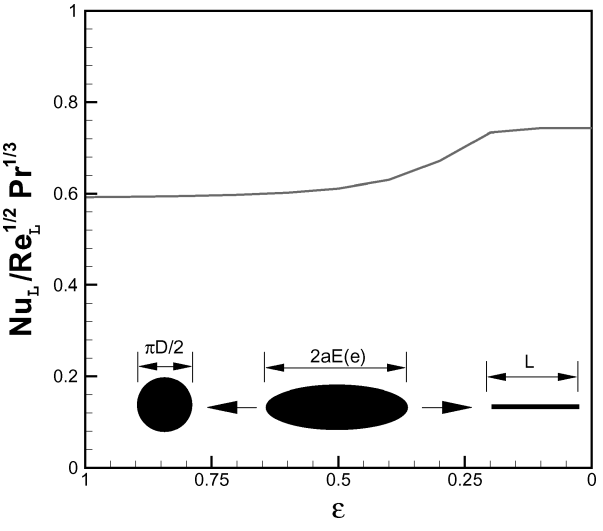

Fig. 6 Variation of heat transfer parameter with axis ratio.

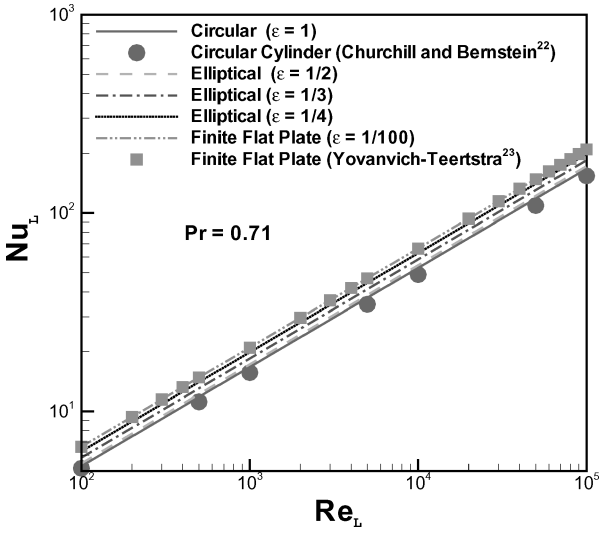

Fig. 7 Variation of average Nusselt number with Reynolds number.

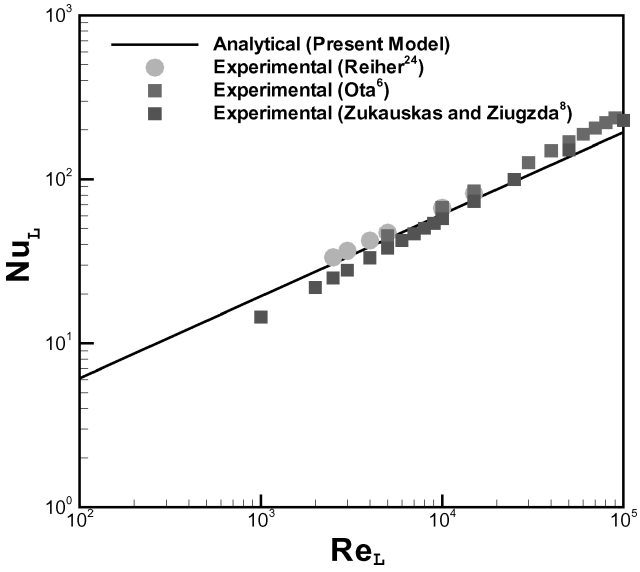

Fig. 8 Variation of average Nusselt number with Reynolds number for elliptic cylinder of axis ratio 1:2.

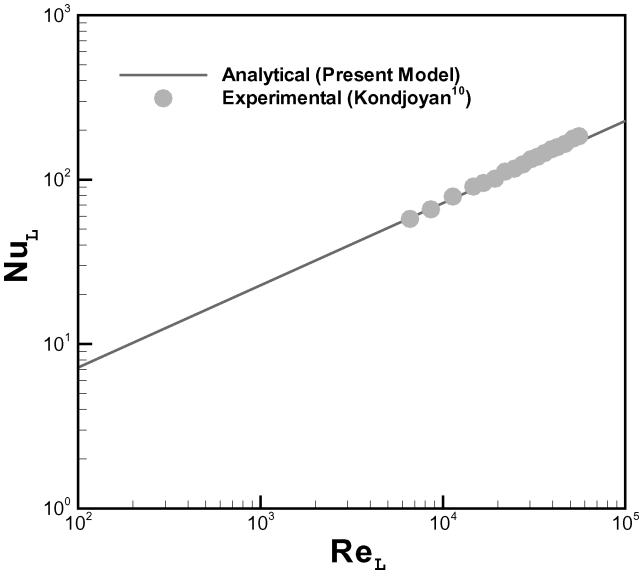

Fig. 9 Variation of average Nusselt number with Reynolds number for isoflux elliptic cylinder of axis ratio 1:4.

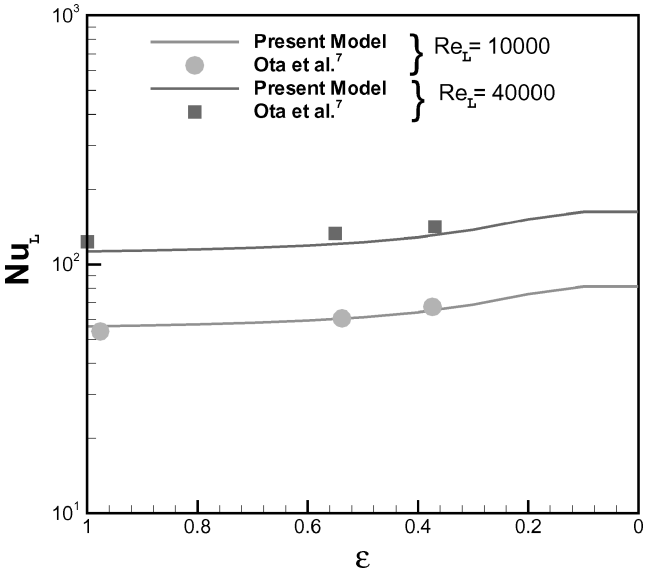

Fig. 10 Variation of average Nusselt number with axis ratio for isoflux elliptic cylinder.

Yovanovich–Teertstra model.[23] It is clear that the present results are in good agreement with the existing data.

The results of heat transfer from a single infinite isoflux elliptical cylinder of axis ratio 1:2 are shown in Fig. 8, where they are compared with the experimental results of Rieher,[24] Ota et al.,[6] and Žukauskas and Žiugžda.[8] Although the Rieher configuration was claimed as obscure by Ota et al.,[6] it shows good agreement with the present results. For the same isoflux boundary condition, the average Nusselt numbers of elliptical cylinders with axis ratios 1:4 are compared with the experimental data of Kondjoyan and Daudin[10] in Fig. 9. It can be seen that $Nu_{\mathcal{L}}$ increases linearly with $Re_{\mathcal{L}}$ on a log–log plot. The present results for elliptical cylinders are in good agreement with the existing data. The variation of average Nusselt numbers of isoflux elliptical cylinders with axis ratio is shown in Fig. 10. The present results are compared with the experimental data of Ota et al.[6,7] for two different Reynolds numbers. The results show good agreement with the experimental data.

Conclusions

Three general correlations, one for drag coefficient and two for heat transfer, have been determined. The drag coefficients are lower, whereas the average heat-transfer coefficients are higher for elliptical cylinders than for circular ones. The effects of the axis ratio of the elliptical cylinder upon drag and the average heat-transfer coefficients are also observed and compared for the two extremes with experimental/numerical values obtained from the open literature. The drag and the average heat-transfer coefficients depend on the Reynolds number as well as the axis ratio.

The present results are in good agreement with the experimental results for the whole laminar range of Reynolds numbers in the absence of freestream turbulence and blockage effects. The correlations obtained in this study can be used to determine the dimensionless drag and heat-transfer coefficients from an elliptical pin fin, where the Reynolds number depends on the characteristic length.

Acknowledgments

The authors gratefully acknowledge the financial support of Natural Sciences and Engineering Research Council of Canada and the Center for Microelectronics Assembly and Packaging.

References

[1]Schubauer, G. B., "Air Flow in a Separating Laminar Boundary Layer," NACA TR-527, Dec. 1934.

[2]Schubauer, G. B., "Air Flow in the Boundary Layer of an Elliptic Cylinder," NACA TR-652, Aug. 1939.

[3]Pohlhausen, K., "Zur Näherungsweise Integration der Differential Gleichung der Laminaren Reibungschicht," *Zeitschrift für angewandte Mathematik und Mechanik*, Vol. 1, 1921, pp. 252–268.

[4]Schlichting, H., and Ulrich, A., "Zur Berechnung des Umschlages Laminar-Turbulent," Jb. dt. Luftfahrtforschung I, Vol. 1, 1942, pp. 8–35.

[5]Schlichting, H., *Boundary Layer Theory*, 7th ed., McGraw–Hill, New York, 1979, Chap. 10.

[6]Ota, T., Aiba, S., Tsuruta, T., and Kaga, M., "Forced Convection Heat Transfer from an Elliptic Cylinder," *Bulletin of the Japan Society of Mechanical Engineers*, Vol. 26, No. 212, 1983, pp. 262–267.

[7]Ota, T., Nishiyama, H., and Taoka, Y., "Heat Transfer and Flow Around an Elliptic Cylinder," *International Journal of Heat and Mass Transfer*, Vol. 27, No. 10, 1984, pp. 1771–1779.

[8]Žukauskas, A., and Žiugžda, J., *Heat Transfer of a Cylinder in Crossflow*, Hemisphere, New York, 1985, Chap. 6.

[9]Modi, V. J., Wiland, E., and Dikshit, A. K., "On the Fluid Dynamics of Elliptic Cylinders," *International Journal of Offshore and Polar Engineering*, Vol. 2, No. 4, 1992, pp. 267–280.

[10]Kondjoyan, A., and Daudin, J. D., "Effects of Free Stream Turbulence Intensity on Heat and Mass Transfers at the Surface of a Circular Cylinder and an Elliptical Cylinder, Axis Ratio 4," *International Journal of Heat and Mass Transfer*, Vol. 38, No. 10, 1995, pp. 1735–1749.

[11]Jackson, C. P., "A Finite-Element Study of the Onset of Vortex Shedding in Flow past Variously Shaped Bodies," *Journal of Fluid Mechanics*, Vol. 182, 1987, pp. 23–45.

[12]D'Allessio, S. J. D., and Dennis, S. C. R., "A Vorticity Model for Viscous Flow past a Cylinder," *Computers and Fluids*, Vol. 23, No. 2, 1994, pp. 279–293.

[13]D'Allessio, S. J. D., and Dennis, S. C. R., "Steady Laminar Forced Convection from an Elliptic Cylinder," *Journal of Engineering Mathematics*, Vol. 29, No. 2, 1995, pp. 181–193.

[14]D'Allessio, S. J. D., "Steady, Unsteady and Linear Stability of Flow past an Elliptic Cylinder," *Canadian Applied Mathematics Quaterly*, Vol. 4, No. 6, 1996, pp. 341–379.

[15]Li, Q., Chen, Z., Flechtner, U., and Warnecke, H. J., "Heat Transfer and Pressure Drop Characteristics in Rectangular Channels with Elliptical Pin Fins," *International Journal of Heat and Fluid Flow*, Vol. 19, No. 3, 1998, pp. 245–250.

[16]Walz, A., "Ein neuer Ansatz für das Greschwindligkeitsprofil der laminaren Reibungsschicht," *Lilienthal-Bericht* 141, 1941, p. 8.

[17]Wieselsberger, C., "New Data on The Laws of Fluid Resistance," NACA TN-84, Vol. 22, 1921.

[18]Janour, Z., "Resistance of a Plate in Parallel Flow at Low Reynolds Number," NACA TM-1316, Nov. 1951.

[19]Dennis, S. C. R., and Dunwoody, J., "The Steady Flow of a Viscous Fluid past a Flat Plate," *Journal of Fluid Mechanics*, Vol. 24, Pt. 3, 1966, pp. 577–595.

[20]Van Dyke, M., *Perturbation Methods in Fluid Mechanics*, Academic Press, New York, 1964, Chap. 7, pp. 121–146.

[21]Kuo, Y. H., "On the Flow of an Incompressible Viscous Fluid past a Flat Plate at Moderate Reynolds Numbers," *Journal of Mathematical Physics*, Vol. 32, 1953, pp. 83–101.

[22]Churchill, S. W., and Bernstein, M., "A Correlating Equation for Forced Convection from Gases and Liquids to a Circular Cylinder in Cross Flow," *Journal of Heat Transfer*, Vol. 99, No. 2, 1977, pp. 300–306.

[23]Yovanovich, M. M., and Teertstra, P., "Laminar Forced Convection from Isothermal Rectangular Plates from Small to Large Reynolds Numbers," *Proceedings of the 7th AIAA/ASME Joint Thermophysics and Heat Transfer Conference*, The Heat Transfer Division, ASME, United Engineering Center, New York, June 1998; also AIAA Paper 98-2675, 1998.

[24]Reiher, H., *Handbuch der Experimentalphysik*, Vol. 9, No. 1, 1925, p. 312.